Investigation of the XCAT phantom as a validation tool in cardiac MRI tracking algorithms

Nicholas Lowther[a,d] , Svenja Ipsen [b,d] , Steven Marsh[a] , Oliver Blanck[c] , Paul Keall[d]
[a]University of Canterbury, Department of Physics and Astronomy, Christchurch, New Zealand
[b]University of Lübeck, Institute for Robotics and Cognitive Systems, Lübeck, Germany
[c]University Medical Center Schleswig-Holstein, Department for Radiation Oncology, Kiel, Germany
[d]University of Sydney, Radiation Physics Laboratory, Sydney, Australia

Keywords

Tracking evaluation, Digital phantom, Cardiac tracking, MRI-guided radiotherapy

Acknowledgements

The authors acknowledge Dr William Paul Segars for providing access to the XCAT phantom. NL disclosed receipt of a Todd Foundation Award for Excellence (Universities New Zealand).

Abbreviations

AF atrial fibrillation

AP anterior posterior

DICOM Digital Imaging and Communications in Medicine

ECG electrocardiogram

FLASH fast low-angle shot

LA left atrium

LR left right

MRI magnetic resonance imaging

MRI-linac MRI linear accelerator

Sis uperior inferior

TrueFISP fast steady-state free precession

XCAT 4D digital extended cardio torso

Abstract

Purpose

To describe our magnetic resonance imaging (MRI) simulated implementation of the 4D digital extended cardio torso (XCAT) phantom to validate our previously developed cardiac tracking techniques. Real-time tracking will play an important role in the non-invasive treatment of atrial fibrillation with MRI-guided radiosurgery. In addition, to show how quantifiable measures of tracking accuracy and patient-specific physiology could influence MRI tracking algorithm design.

Methods

Twenty virtual patients were subjected to simulated MRI scans that closely model the proposed real-world scenario to allow verification of the tracking technique's algorithm. The generated phantoms provide ground-truth motions which were compared to the target motions output from our tracking algorithm. The patient-specific tracking error, e_p, was the 3D difference (vector length) between the ground-truth and algorithm trajectories. The tracking errors of two combinations of new tracking algorithm functions that were anticipated to improve tracking accuracy were studied. Additionally, the correlation of key physiological parameters with tracking accuracy was investigated.

Results

Our original cardiac tracking algorithm resulted in a mean tracking error of 3.7 ± 0.6 mm over all virtual patients. The two combinations of tracking functions demonstrated comparable mean tracking errors however indicating that the optimal tracking algorithm may be patient-specific.

Conclusions

Current and future MRI tracking strategies are likely to benefit from this virtual validation method since no time-resolved 4D ground-truth signal can currently be derived from purely image-based studies.

1. Introduction

Magnetic resonance imaging (MRI)-based tracking strategies for the use in emerging MRI-guided radiotherapy systems have demonstrated the ability to precisely localize and follow organ and tumor position in real-time scenarios [1,2]. Ideally, these tracking applications would utilize MRI sequences that can acquire time-resolved target volumes in real-time (4D). However, this is often restricted due to the complexities of 4D-MRI [3]. A number of recent studies utilize real-time interleaved orthogonal 2D cine-MRI slices [4-7] to provide real-time information about the target position in an effort to compensate for the lack of real 4D MRI data. Template matching [8, 9] is a common localization technique where a previously acquired volume-of-interest is matched to a target image, in this case fast acquired 2D MRI planes. Other localization strategies utilizing orthogonal MRI focus on automatic feature extraction for motion prediction [10,11].

A recent study by Ipsen et al. [12] suggested that a non-invasive treatment of atrial fibrillation (AF), the most common cardiac arrhythmia with millions of patients worldwide [13], could be facilitated by using an MRI linear accelerator (MRI-linac) with real-time image guidance. Despite the spatial and temporal limitations of 4D-MRI for this purpose, a guidance method incorporating a cardiac tracking algorithm was developed. Similar to previous approaches [2], [8] the target, i.e. the left atrium (LA), and its 3D position during the proposed radiosurgery is detected through template matching of a pre-treatment target volume to orthogonal real-time planes [14]. Orthogonal real-time planes are used in an effort to provide adequate positional information in all anatomical planes (i.e. sagittal, coronal, axial). The temporal acquisition times of the real-time planes are more appropriate than that of complete 3D MRI volumes when tracking complex cardiac and respiratory motion. The template matching calculates similarity between the target volume image and the real-time planes to assign ‘best-match’ 3D positions during the proposed treatment. To account for the rapid target deformations caused by the heartbeat, an electrocardiogram (ECG) surrogate and a multi-phase template were incorporated into the method. The ECG signal determines which pre-treatment template will be used in the matching process.

New tracking strategies, such as our cardiac tracking algorithm, could directly improve treatment quality due to their ability to visualize internal moving organs in real-time with superior soft-tissue contrast and without using ionizing radiation. However, in a clinical scenario the economic and time-related burdens on specialists, patients and departments do not always allow rigorous testing of every new method on real patient data. It would be beneficial to assess the accuracy of a specific tracking technique and investigate the influence of different anatomical parameters on the approach before moving towards clinical implementation and patient studies. This is particularly relevant in developing MRI integrated radiotherapy units [15,16] where a number of image-guided treatment scenarios have been proposed [7, 17]. Physical phantoms could be an alternative but are restricted in their modeling of realistic patient physiology, especially reproducible deformation, and fabrication cost. The previously described lack of real-time volumetric MRI data increases the challenge of validating the accuracy of MRI tracking strategies in general since a time-resolved ground-truth can merely be approximated.

Digital phantoms allow simulation of realistic patient anatomy and physiology. They also provide a desirable tool in exploring and developing novel image interpretations studies because of the known and quantifiable 4D phantom anatomy. A number of digital phantoms have been developed for use in medical imaging analysis [18-22]. Organ-specific digital phantoms [21, 22] are generally designed for a specific image analysis investigation, restricting their use as a tool in tracking validations of multi-organ systems. In contrast, the 4D digital extended cardio torso (XCAT) phantom [19, 20] has the ability to model a wide range of patient anatomies, provides a realistic interaction of multiple organs and a multitude of simulated imaging modalities. These design features of the XCAT phantom, described in detail in the literature [19, 20], make it a suitable validation tool for various tracking applications. The XCAT phantom has been used periodically in experimental investigations, e.g. to simulate realistic cardiac MRI on a virtual patient cohort of 40 digital phantoms [23], for the modeling of regional heart defects caused by ischemia with incorporation of a finite-element model [24] and in respiration-focused modeling applications. The respiration-focused modeling applications include the verification of

reproducible patient-specific diaphragm and chest motion traces for lung cancer radiotherapy [25], the validation of novel 4D-MRI techniques which image respiratory motion [26] and an analysis of audiovisual biofeedback and gating on thoracic-abdominal 4D computed tomography [27].

In Ipsen et al. [14] the XCAT phantom was first utilized to validate the MRI cardiac tracking algorithm by comparing the developed method's target trajectories with a ground-truth trajectory output from the XCAT phantom. Here, we now describe in detail the implementation of the XCAT phantom to validate and assess our cardiac tracking techniques and show how this quantifiable measure of tracking accuracy and patient-specific physiology could influence and improve MRI tracking algorithm design.

2. Methods and materials

2.1. Virtual patient dataset

To cover a range of different patient anatomies we generated a virtual dataset of 20 patients by using different XCAT phantom parameter sets and utilized the digital phantom's ability to control anatomical and physiological parameters, in addition to its MRI simulation capabilities. Six specific anatomical parameters of the XCAT's initialization file were anticipated to strongly influence algorithmic tracking robustness and were varied across the 20 virtual patients. These were LA volume, heart rate, respiratory rate and cardiac respiratory motion broken into its three constituent components – superior inferior (SI), anterior posterior (AP) and left right (LR). The three motion-related parameters (heart rate, respiratory rate and respiratory motion) can be manipulated directly in the XCAT parameter initialization file while the LA volume was controlled indirectly by either scaling the entire phantom or scaling the heart only. Both scaling factors were varied for all 20 virtual patients in the XCAT parameter initialization file

To date, only healthy volunteers have been included in our cardiac tracking research [12, 14]. For comparability, the virtual dataset was designed to replicate this digitally. Anatomical parameters of the virtual patients were randomly generated based on distributions (mean and sample standard deviation) from our previous studies [12, 14], and taken from literature when appropriate data was unavailable. The reference values and sources are shown in Table 1. The individual XCAT patients' parameters are shown in Table 2.

2.2. Simulated MRI scans

Virtual phantoms were generated to validate our cardiac MRI tracking algorithm using the XCAT's activity mode [20]. Pixel intensities of organs and tissues were assigned values based on the image data acquired using a fast steady-state free precession (TrueFISP) sequence from our previous study [14]. The conversion of XCAT raw binary files into Digital Imaging and Communications in Medicine (DICOM) format and the subsequent validation of the tracking algorithm were conducted with in-house developed software (MATLAB 2014b version 8.4, The MathWorks Inc.). Assessment of our real-time LA localization strategy based on template matching with MRI required the generation of three phantoms for each of the 20 virtual patients, shown in Fig. 1.

2.3. Phantoms for template generation

Two static phantoms (i.e. 3D) were generated at end-exhale for atrial systole and end-diastole to simulate the dual-phase template combination of our previous work [14]. The respiratory motion component was eliminated to mimic image acquisition during breath-hold. The phantoms were generated with regular (i.e. non-arrhythmic) anatomical parameters and with isotropic voxels of 1.3 mm to match the in-plane pixel size of the TrueFISP breath-hold scans. Partial volume artifacts were introduced by combining four adjacent sagittal slices and averaging their voxel intensities. This combination took place successively across the lateral span of the phantom. These combined slices more accurately represented the real-world MRI slice thickness (i.e. 5.2 mm) based on previous experiences. The simulated 2D MRI scan parameters are shown in Table 3. A 3D template

volume was created by delineating the desired target structure (LA) in each 2D slice that contained the anatomical structure. By definition, the XCAT phantom produces homogeneous voxel values for each specified organ/region. The homogeneous voxel value, or so-called 'activity unit' for the LA was assigned in the XCAT's parameter initialization file and was non-identical to other organs/regions We ran a simple binary algorithm over the phantom for template generation to isolate those voxels associated with the LA's activity unit. By performing an automatic pixel thresholding of the intended LA target, the final 3D volume template was extracted. This method was validated by comparing the Dice similarity coefficient (DSC) [30] of the template volume and the LA of the phantom. As expected, there was perfect overlap (i.e. DSC = 1). The automatic nature of the segmentation as opposed to a manual delineation is advantageous in a validation method for tracking accuracy since no areas of the LA target are missed (template LA dimensions are identical to the XCAT's raw data LA dimensions) and the undesired inter-/intra-user variability is removed. This process was repeated on both atrial phase phantoms.

2.4. Real-time image phantom

In the cardiac tracking algorithm, the 3D target templates are being matched to orthogonal 2D real-time planes. A phantom was generated using the same anatomical parameters as for the phantoms used for the 3D target volume generation. However, this dynamic phantom (i.e. 4D) included free breathing motion. The real-time images were extracted at specified time intervals throughout the 4D phantom. The interleaved real-time acquisition scheme was simulated by extracting three slices centered about the LA at 200 ms intervals for both orthogonal orientations (sagittal and coronal) from the dynamic phantom. The phantom was generated with isotropic voxels of 2.0 mm to match the in-plane pixel size of the TrueFISP 2D-2D scans. The real-time scan parameters of the simulated sequence are shown in Table 3.

Partial volume artifacts were included, with sagittal and coronal real-time planes being the mean pixel intensity of the central and two adjacent slices (i.e. the three extracted slices) to give a slice thickness representative of the real-world workflow (i.e. 6 mm). Furthermore, Gaussian noise was added in the real-time scans [31]. The power of the noise was estimated from the standard deviation of the pixel intensity of a region with no signal from the real-time images of our previous study [14]. Gaussian noise was not added in the phantoms for template generation due to its incompatibility with automatic delineation. Fig. 2 shows a volunteer scan from our previous cardiac tracking study [14] with simulated sagittal real-time planes using the XCAT phantom exclusive and inclusive of partial volume and noise artifacts.

2.5. Validation of the original and extended tracking algorithms

Initially, we tracked the LA target in all generated virtual phantoms (n = 20) using the original real-time tracking algorithm [14] which outputs target motion trajectories in three anatomical axes (SI, AP, LR). Target motion is inferred from the volumetric center coordinate of the template's bounding box.

The ground-truth target trajectory was calculated in each real-time frame for the virtual phantom as the LA's bounding box center coordinate. The LA volume was isolated with voxel intensity thresholding, visualized in Fig. 3. An individual patient's tracking error ep was calculated as the mean of the 3D vectors of the difference between the matched position (Mx,My,Mz) and ground truth position (Gx,Gy,Gz) for each time frame t, over all time frames T:

$$e_p = \frac{1}{T}\sum_{t=1}^{T}\sqrt{\left(Mx_{t,p} - Gx_{t,p}\right)^2 + \left(My_{t,p} - Gy_{t,p}\right)^2 + \left(Mz_{t,p} - Gz_{t,p}\right)^2}$$

For *P* virtual patients, the mean of all patients' individual tracking errors e provided an overall metric to assess the tracking accuracy of the original and extended algorithms:

$$e = \frac{1}{P}\sum_{p=1}^{P} e_p$$

2.6. Extension of the tracking algorithm

The quantitative error measure facilitated iterative development of the MRI tracking algorithm in an effort to increase the tracking accuracy. Three new tracking functionalities were implemented into the tracking algorithm with inter-functional compatibility included in their design, where appropriate. An all positions (APS) function iteratively passed each segmented plane of the template volume over the 2D real-time plane in an effort to find a best match location. In comparison, the original tracking method followed an approach where the current 2D match plane of the template is selected from the last position (LP) best match recorded on an orthogonal plane [14], therefore not searching the entire template volume. A bordered template (BT) function allowed a user definable number of blank voxels void of target volume but containing the adjacent anatomy to the outside of the 3D template volume. In an effort to increase tracking robustness, a dynamic search (DS) function was implemented where successive matching locations could only be located within a user defined distance, guided by observed and known LA motion trajectories [32]. Two specific combinations of the tracking algorithm's new functions and that were anticipated to improve tracking accuracy were tested on the 20 virtual patients. Combination 1 incorporated the LP, BT and DS functions while combination 2 incorporated the APS, BT and DS functions. A patient-specific tracking accuracy was recorded for each combination.

2.7. Spatial resolution manipulation and artifact reduction

To test if a reduction in through-plane slice thickness and artifact reduction would lead to improved tracking accuracy the entire target volume procedure was repeated with isotropic voxels of 2 mm for the respective 2D images, however with the removal of partial volume effects. The isotropic voxels resulted in a decrease of spatial resolution detail from 1.3 mm to 2 mm for the in-plane pixels of cardiac template images. The flexibility of our tracking algorithm allowed original and spatially manipulated images to be used interchangeably.

2.8. Tracking error correlation with physiological parameters

For the original tracking algorithm, Pearson correlation coefficients were conducted between the individual tracking errors and six physiological parameters: LA volume, heart rate, respiratory rate and cardiac respiratory motion broken into its three constituent components (SI, AP, LR). The p-values for the Pearson correlation coefficients were calculated using a Student's t-distribution. This study was the first to investigate whether variation of anatomical parameters correlated significantly with tracking error and as such, $p < .008$ was considered statistically significant after a Bonferroni correction (from $\alpha = 0.05$). A sample size of $n = 13$ virtual patients was sufficient at the 0.80 level of power.

3. Results

3.1. Tracking accuracy of the original and extended tracking algorithms

The 3D tracking error of the original tracking algorithm over all 20 virtual patients was 3.7 ± 0.6 mm (mean ± std).

Tracking errors across the 20 virtual patients for the two new function combinations and spatial manipulation test are shown in Fig. 4. While the tracking accuracy for the 20 virtual patients remained relatively unchanged by applying different combinations of extensions of the original tracking algorithm, an individual patient's tracking error did not necessarily follow this trend, which reflected in the patient-specific tracking errors in Fig. 4. The optimal tracking function combination was therefore patient-specific as was the lowest achievable

tracking error. However, statistical comparison between the four different tracking functions did not result in significant differences.

Fig. 5 shows representative comparisons between ground-truth patient trajectories and the output of the original tracking algorithm for a best, average and worst case tracking performance. The high frequency components in the ground-truth directions are caused by the periodic cardiac contraction while the low frequency components are due to the respiratory motion during real-time acquisition. It can be seen that the tracking algorithm follows the LA motion accurately most of the time. Large-magnitude respiratory motion was detected robustly. The rapid contractile motion component appears to be more difficult to track and some outliers and non-matches occur. Relative to respiratory motion magnitude, large contraction motion magnitudes in both the AP and LR planes reduce tracking robustness, as illustrated in Fig. 5 (c). In Fig. 5(a), only the LR motion exhibits this property and the tracking robustness is not compromised. These individual patients' physiological parameters and tracking accuracy are shown in Table 4. Relative to the other virtual patients, a best case generally displayed low magnitude and frequency of respiratory and cardiac cycles while a worst case exhibited higher magnitude and frequency.

3.2. Anatomical parameter analysis

For the six varied anatomical parameters tested here, none correlated significantly with tracking accuracy as shown in Table 5. A faster heart rate was not definitively associated with a decrease in tracking accuracy. An increase in LA volume did not correspond to an improved tracking accuracy, contrary to what was anticipated when using a larger template registration area. Increases in respiratory rate and the cardiac respiratory motion's three constituent components; SI, AP and LR did not result in a significant reduction of the tracking accuracy.

4. Discussion

Using the virtual XCAT patients our original tracking algorithm resulted in a mean 3D tracking error of 3.7 ± 0.6 mm. To be consistent with the error quantification method of other tracking studies [2], [10], the individual patient error metric was modified in this study. Instead of the previously utilized 3D vector of the mean differences between the tracking algorithm and ground-truth anatomical plane trajectories in each anatomical plane [14], the mean of the 3D differences (vector lengths) for each real-time match was calculated. The change in metric changed the mean tracking accuracy over all virtual patients from 3.2 ± 1.7 mm to 3.7 ± 0.6 mm.

The developed validation procedure allowed an easy implementation of additional algorithmic functionality, both on the algorithm and the image resolution side. However, the mean tracking accuracy was largely unchanged. The dynamic search function included in tracking "Combination 1" successfully removed matches which could be considered outliers and slightly improved the tracking accuracy of patients 1, 4 and 5 as shown in Fig. 4. For the "Last Position" functionality, the current 2D match plane of the template is selected from the last position best match recorded on an orthogonal plane. When changing between templates, a best match location on a diastole template does not necessarily correspond to the same location on a systole template as the two are related through a non-rigid deformation. This work suggests that the last position functionality limits tracking accuracy. However, in an "All Positions" scenario, the increased number of possible match planes increases the chance of an incorrect match location. The potential of using a 4D template solution to overcome these limitations will be investigated in the future.

The proposed tracking algorithm tackles a more difficult 4D problem than existing algorithms which track only in-plane motion or only respiratory motion, Cerviño et al. [10] produced a mean tracking error of 0.4 mm when tracking visible vascular structures of the lung in a free breathing environment using single 2D cine-MRI sagittal images. It is important to note that this study did not include out-of-plane motion. Bjerre et al. [2] demonstrated 3D tracking of the kidney with an accuracy slightly over 1 mm when utilizing a 3D-2D approach similar to the tracking workflow presented in our study. However, none of these studies dealt with the much

faster and more complex cardiac motion. The difference in accuracies is likely caused by the incomparable anatomical locations.

For AF treatment plans, margin sizes less than 3–5 mm may be within acceptable limits [12], [33]. Therefore, the tracking error of the tracking algorithm in our study (3.7 ± 0.6 mm) could contribute to the proof-of-concept for non-invasive cardiac radiosurgery under real-time MRI guidance. However, improvements to the algorithm are the subject of ongoing research in order to further reduce the tracking error.

In comparison to other studies which utilize the XCAT for simulation studies [26, 34], we demonstrated how differing patient physiology could influence tracking accuracy. For the 20 virtual patients studied, the heart rate was the most influential anatomical parameter affecting the tracking accuracy. Acquisition times of 200 ms may indicate that for fast beating hearts, a significant amount of information was lost between real-time planes. Advances in real-time MRI using radial fast low-angle shot (FLASH) techniques have allowed for much shorter acquisition times [35-37] than used in our proposed MRI workflow. In this case, information regarding a rapid heart cycle for use in our tracking algorithm would be adequately acquired with a higher temporal resolution. We anticipate the increase in real-time image temporal resolution would lead to a lower tracking error, which is under further investigation. Slice thickness is slightly increased in FLASH images, but this work has shown that tracking errors of the virtual patient investigations were largely unchanged with varied spatial resolution.

Overall, the results of our work lead us to hypothesize that tracking algorithms for MRI-guided radiotherapy could benefit from the validation methodology used in this work: we provided a ground truth comparison and removed study recruitment burdens without the adding to departmental workload. This is further demonstrated through a number of studies that have attempted to evaluate MRI tracking algorithms for lung cancer applications [9, 38, 39]. Shi et al. [9] showed that the performance of an automated template matching algorithm had localization accuracy comparable or better than manual delineation however, this was established by a trained physician in each real-time frame. Furthermore, this algorithm and subsequent evaluation was developed for lung tumor tracking in 2D and did not account for motion orthogonal to the target image, characteristic of in vivo evaluation studies and MRI-linac motion compensation strategies to date. In comparison to these, our validation is not restricted by this out-of-plane motion. Furthermore, our method is not limited by physician delineation time, externally-based phantoms or patient/volunteer recruitment burdens. This method of validation could be extended to algorithms that track areas of non-rigid motion in the lung, such as tumors in near proximity to the heart wall [40] that experience pulsatile motion. Although not detailed in this work, we expect that this validation method could be used for a range of tracking validations and treatment planning studies, especially when 4D patient data is difficult to acquire. In fact, imaging data comprising cardiac and respiratory motion alike would have been helpful in previous treatment planning studies for cardiac radiosurgery [12, 33]. The analysis in this work was made possible by validation through quantitative measures provided by the XCAT digital phantom for the first time.

Despite the realistic simulations the XCAT phantom's most obvious limitation is its digital nature. Tissue appearance, tissue motion and imaging modality replication are areas where the XCAT realism could be improved. Each anatomical structure is modeled in a homogeneous manner, organs and their sub-structures are of the same pixel value. As a result, image artifacts due to tissue heterogeneity are not simulated realistically. In our validation procedure, partial volume and noise artifacts were added manually.

Our XCAT study also assumed constant respiratory cycle lengths and heart rates and does not factor any intra-treatment variation. However, the tracking algorithm performs a new localization search with every real-time plane so motion trajectory variability is not anticipated to adversely affect tracking accuracy. Additionally,

deformation to the heart from respiratory influences [41] was not fully considered as the templates are derived from phantoms at full exhale. Deformation to the templates from any other phase of the respiratory cycle was not considered. Further to this, the XCAT templates are automatically delineated on the same 'breath-hold' phantom and hence achieve perfect alignment. In the real-world procedure the breath-hold nature of the template scans can lead to geometric misalignment for the templates.

As a consequence, the XCAT must be considered an idealized scenario. However, the virtual study demonstrates the usability of data when testing and refining tracking algorithms within a model scenario, which is desirable in the wider context of image-guided radiotherapy and radiosurgery. Future versions of the XCAT phantom will minimize the current limitations and further promote its use in validating image simulation strategies.

5. Conclusion

We have developed a method of validation for tracking algorithms and applied it to an existing localization method for real-time MRI-guided cardiac radiosurgery. The XCAT phantom software was chosen due to the common problem of unavailability of real-time anatomical imaging data including respiratory and cardiac motion. The presence of a quantitative measure against the ground-truth allowed the investigation of the influence of patient-specific anatomical and physiological parameters on tracking performance and helped us to improve our tracking algorithms. Current and future MRI tracking strategies and various other applications are likely to benefit from this virtual validation.

References

[1] Brix L, Ringgaard S, Sørensen TS, Poulsen PR. Three-dimensional liver motion tracking using real-time two-dimensional MRI. Med Phys 2014;41:42302.

[2] Bjerre T, Crijns S, af Rosenschöld PM, Aznar M, Specht L, Larsen R, et al. Three dimensional MRI-linac intra-fraction guidance using multiple orthogonal cine-MRI planes. 2013;58:4943.

[3] Li G, Citrin D, Camphausen K, Mueller B, Burman C, Mychalczak B, et al. Advances in 4D medical imaging and 4D radiation therapy. Technol Cancer Res Treat 2008;7:67–81.

[4] Harris W, Ren L, Cai J, Zhang Y, Chang Z, Yin F-F. A technique for generating volumetric cine-magnetic resonance imaging. Int J Radiat Oncol Biol Phys 2016;95:844–53.

[5] Paganelli C, Lee D, Greer PB, Baroni G, Riboldi M, Keall P. Quantification of lung tumor rotation with automated landmark extraction using orthogonal cine MRI images. Phys Med Biol 2015;60:7165.

[6] Seregni M, Paganelli C, Lee D, Greer PB, Baroni G, Keall PJ, et al. Motion prediction in MRI-guided radiotherapy based on interleaved orthogonal cine-MRI. Phys Med Biol 2016;61:872.

[7] Stemkens B, Tijssen RH, de Senneville BD, Lagendijk JJ, van den Berg CA. Image driven, model-based 3D abdominal motion estimation for MR-guided radiotherapy. Phys Med Biol 2016;61:5335.

[8] Tryggestad E, Flammang A, Hales R, Herman J, Lee J, McNutt T, et al. 4D tumor centroid tracking using orthogonal 2D dynamic MRI: Implications for radiotherapy planning. Med Phys 2013;40:91712.

[9] Shi X, Diwanji T, Mooney KE, Lin J, Feigenberg S, D'Souza WD, et al. Evaluation of template matching for tumor motion management with cine-MR images in lung cancer patients. Med Phys 2014;41:52304.

[10] Cerviño LI, Du J, Jiang SB. MRI-guided tumor tracking in lung cancer radiotherapy. Phys Med Biol 2011;56:3773.

[11] Paganelli C, Seregni M, Fattori G, Summers P, Bellomi M, Baroni G, et al. Magnetic resonance imaging–guided versus surrogate-based motion tracking in liver radiation therapy: a prospective comparative study. Int J Radiat Oncol Biol Phys 2015;91:840–8.

[12] Ipsen S, Blanck O, Oborn B, Bode F, Liney G, Hunold P, et al. Radiotherapy beyond cancer: target localization in real-time MRI and treatment planning for cardiac radiosurgery. Med Phys 2014;41:120702.

[13] Ball J, Carrington M, McMurray J, Stewart S. Atrial fibrillation: profile and burden of an evolving epidemic in the 21st century. Int J Cardiol 2013;167:1807–24.

[14] Ipsen S, Blanck O, Lowther NJ, Liney GP, Rai R, Bode F, et al. Towards real-time MRI-guided 3D localization of deforming targets for non-invasive cardiac radiosurgery. Phys Med Biol 2016;61:7848.

[15] Keall PJ, Barton M, Crozier S. The Australian magnetic resonance imaging-linac program. 2014;24:203–6. Elsevier.

[16] Lagendijk JJ, Raaymakers BW, van Vulpen M. The magnetic resonance imaginglinac system. 2014;24:207–9. Elsevier.

[17] Yun J, Wachowicz K, Mackenzie M, Rathee S, Robinson D, Fallone BG. First demonstration of intrafractional tumor-tracked irradiation using 2D phantom MR images on a prototype linac-MR. Med Phys 2013;40:51718.

[18] Zubal IG, Harrell CR, Smith EO, Rattner Z, Gindi G, Hoffer PB. Computerized threedimensional segmented human anatomy. Med Phys 1994;21:299–302.

[19] Segars WP, Mahesh M, Beck TJ, Frey EC, Tsui BM. Realistic CT simulation using the 4D XCAT phantom. Med Phys 2008;35:3800–8.

[20] Segars WP, Sturgeon G, Mendonca S, Grimes J, Tsui BM. 4D XCAT phantom for multimodality imaging research. Med Phys 2010;37:4902–15.

[21] Kudo K, Christensen S, Sasaki M, Østergaard L, Shirato H, Ogasawara K, et al. Accuracy and reliability assessment of CT and MR perfusion analysis software using a digital phantom. Radiology 2013;267:201–11.

[22] Zhong H, Kim J, Chetty IJ. Analysis of deformable image registration accuracy using computational modeling. Med Phys 2010;37:970–9.

[23] Tobon-Gomez C, Sukno FM, Bijnens BH, Huguet M, Frangi AF. Realistic simulation of cardiac magnetic resonance studies modeling anatomical variability, trabeculae, and papillary muscles. Magn Reson Med 2011;65:280–8.

[24] Veress AI, Segars WP, Tsui BM, Gullberg GT. Incorporation of a left ventricle finite element model defining infarction into the XCAT imaging phantom. IEEE Trans Med Imaging 2011;30:915–27.

[25] Cai J, Chang Z, Wang Z, Segars WP, Yin F-F. Four-dimensional magnetic resonance imaging (4D-MRI) using image-based respiratory surrogate: a feasibility study. Med Phys 2011;38:6384–94.

[26] Liu Y, Yin F-F, Rhee D, Cai J. Accuracy of respiratory motion measurement of 4DMRI: a comparison between cine and sequential acquisition. Med Phys 2016;43:179–87.

[27] Pollock S, Kipritidis J, Lee D, Bernatowicz K, Keall P. The impact of breathing guidance and prospective gating during thoracic 4DCT imaging: an XCAT study utilizing lung cancer patient motion. Phys Med Biol 2016;61:6485. http://dx.doi. org/10.1088/0031-9155/61/17/6485.

[28] Hudsmith LE, Petersen SE, Francis JM, Robson MD, Neubauer S. Normal human left and right ventricular and left atrial dimensions using steady state free precession magnetic resonance imaging. J Cardiovasc Magn Reson 2005;7:775–82.

[29] Barrett KE, Barman SM, Boitano S, et al. Ganong's review of medical physiology. New Delhi: McGraw Hill; 2010. p. 2010.

[30] Zou KH, Warfield SK, Bharatha A, Tempany CMC, Kaus MR, Haker SJ, et al. Statistical validation of image segmentation quality based on a spatial overlap index: scientific reports. Acad Radiol 2004;11:178–89.

[31] Gudbjartsson H, Patz S. The Rician distribution of noisy MRI data. Magn Reson Med 1995;34:910–4.

[32] Ector J, De Buck S, Loeckx D, Coudyzer W, Maes F, Dymarkowski S, et al. Changes in left atrial anatomy due to respiration: impact on three-dimensional image integration during atrial fibrillation ablation. J Cardiovasc Electrophysiol 2008;19:828–34. http://dx.doi.org/10.1111/j.1540-8167.2008.01128.x.

[33] Blanck O, Ipsen S, Chan MK, Bauer R, Kerl M, Hunold P, et al. Treatment Planning Considerations for Robotic Guided Cardiac Radiosurgery for Atrial Fibrillation. Cureus n.d.; 8. http://dx.doi.org/10.7759/cureus.705.

[34] Panta RK, Segars P, Yin F-F, Cai J. Establishing a framework to implement 4D XCAT Phantom for 4D radiotherapy research. J Cancer Res Ther 2012;8:565.

[35] Uecker M, Zhang S, Voit D, Karaus A, Merboldt K-D, Frahm J. Real-time MRI at a resolution of 20 ms. NMR Biomed 2010;23:986–94.

[36] Voit D, Zhang S, Unterberg-Buchwald C, Sohns JM, Lotz J, Frahm J. Real-time cardiovascular magnetic resonance at 1.5 T using balanced SSFP and 40 ms resolution. J Cardiovasc Magn Reson 2013;15:1.

[37] Joseph AA, Merboldt K-D, Voit D, Zhang S, Uecker M, Lotz J, et al. Real-time phasecontrast MRI of cardiovascular blood flow using undersampled radial fast low-angle shot and nonlinear inverse reconstruction. NMR Biomed 2012;25:917–24.

[38] Du J, Jiang SB, et al. MRI-guided tumor tracking in lung cancer radiotherapy. Phys Med Biol 2011;56:3773.

[39] Yun J, Yip E, Wachowicz K, Rathee S, Mackenzie M, Robinson D, et al. Evaluation of a lung tumor autocontouring algorithm for intrafractional tumor tracking using low-field MRI: a phantom study. Med Phys 2012;39:1481–94.

[40] Seppenwoolde Y, Shirato H, Kitamura K, Shimizu S, van Herk M, Lebesque JV, et al. Precise and real-time measurement of 3D tumor motion in lung due to breathing and heartbeat, measured during radiotherapy. Int J Radiat Oncol Biol Phys 2002;53:822–34.

[41] McLeish K, Hill DL, Atkinson D, Blackall JM, Razavi R. A study of the motion and deformation of the heart due to respiration. IEEE Trans Med Imaging 2002;21:1142–50.

Table 1. Reference values and sources for the physiological parameters of the 4D extended cardiac-torso (XCAT) virtual study.

Parameter	Reference value (mean ± SD)	Reference source
LA max-diastolic volume (ml)	103 ± 30	Hudsmith et al. [28]
Heart rate (bpm)	58.3 ± 10.3	ECG data from our scanned volunteers [12], [14]
Respiratory rate (cycles per min)	13.5 ± 1.5	Ganong and Barrett [29]
LA respiratory motion LR (mm)	3.1 ± 1.1	Ipsen et al. [14]
LA respiratory motion AP (mm)	5.8 ± 3.5	Ipsen et al. [14]
LA respiratory motion SI (mm)	16.5 ± 8.0	Ipsen et al. [14]

Table 2. Individual physiological parameter values of the 20 4D extended cardiac-torso (XCAT) virtual patients.

Patient	Maximal LA volume (ml)	LA respiratory motion			Heart rate (bpm)	Respiratory rate (cycles per min)
		AP (mm)	LR (mm)	SI (mm)		
1	73.1	14.0	1.2	27.0	65	14.4
2	88.6	10.1	2.7	16.7	66	15.2
3	104.8	1.0	4.9	15.6	75	13.1
4	92.1	8.5	2.1	25.5	59	13.9
5	104.0	6.5	5.2	9.6	68	11.5
6	79.5	8.5	2.6	12.0	54	15.5
7	102.2	7.2	1.2	14.8	42	10.8
8	77.3	2.7	4.0	11.8	64	13.0
9	69.0	6.8	2.7	23.1	69	16.5
10	103.5	7.4	3.5	23.5	64	12.0
11	119.8	5.8	2.5	8.4	48	13.2
12	55.2	7.1	3.3	16.9	50	11.6
13	89.7	2.9	3.9	9.3	56	13.0
14	122.6	14.7	4.2	15.5	54	10.5
15	49.4	1.8	2.5	17.2	79	14.6
16	94.6	6.4	4.5	26.7	78	13.6
17	103.5	8.8	3.9	11.9	64	12.5
18	82.7	0.7	2.1	22.9	48	12.7
19	90.9	4.7	2.6	4.6	55	13.8
20	71.0	11.1	3.3	19.2	60	15.6

Table 3. The simulated MRI parameters for the 3D breath-hold planning and 2D-2D real-time scans conducted on the twenty 4D extended cardiac-torso (XCAT) virtual patients.

Parameter	**3D breath-hold planning scan**	**2D-2D orthogonal real-time scan**
Scan direction	Sagittal	Sagittal – coronal
In-plane pixel size	1.3 mm	2 mm
Slice thickness	5.2 mm	6 mm
Field-of-view	318.5 mm^2	320 mm^2
Cardiac phases	Systole/end-diastole	–
Temporal resolution	–	200 ms

Table 4. Individual anatomical parameters and tracking error for the best, average and worst case virtual patients.

Virtual patient	**Maximal LA volume (ml)**	**AP (mm)**	**LA respiratory motion LR (mm)**	**SI (mm)**	**Heart rate (bpm)**	**Respiratory rate (cycles per min)**	**Tracking error e_p(mm)**
12 (Best case)	55.2	7.1	3.3	16.9	50	11.6	2.4
14 (Average case)	122.6	14.7	4.2	15.5	54	10.5	3.6
16 (Worst case)	94.6	6.4	4.5	26.7	78	13.6	5.4

Table 5. Pearson correlation coefficient r and p-values for tracking accuracy against the physiological parameters of the 4D extended cardiac-torso (XCAT) virtual study.

Anatomical parameter	***r***	***p***
LA max-diastolic volume	0.31	0.19
Heart rate	0.54	0.014
Respiratory rate	-0.03	0.90
LA respiratory motion LR	0.28	0.24
LA respiratory motion AP	-0.18	0.46
LA respiratory motion SI	0.31	0.19

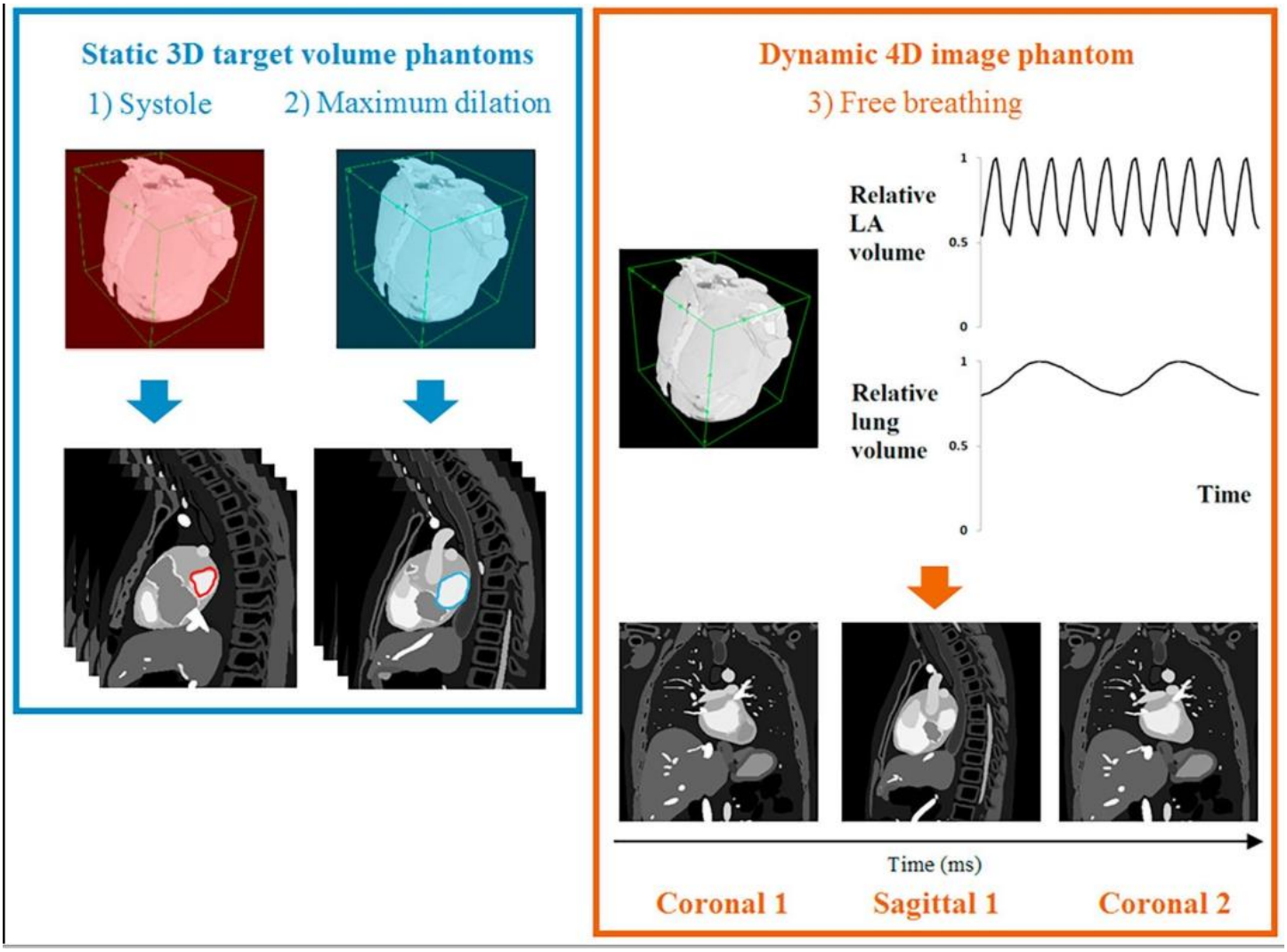

Fig. 1. Three phantoms were generated for each of the 20 virtual patients. Two static 3D end-exhale phantoms, one at atrial systole and one at atrial end-diastole (left), were used to delineate the 3D templates from each 2D slice containing left atrium target volume. The third phantom, a dynamic 4D phantom representing a free breathing scenario (right) was generated and orthogonal "real-time" slices were extracted at 200 ms intervals.

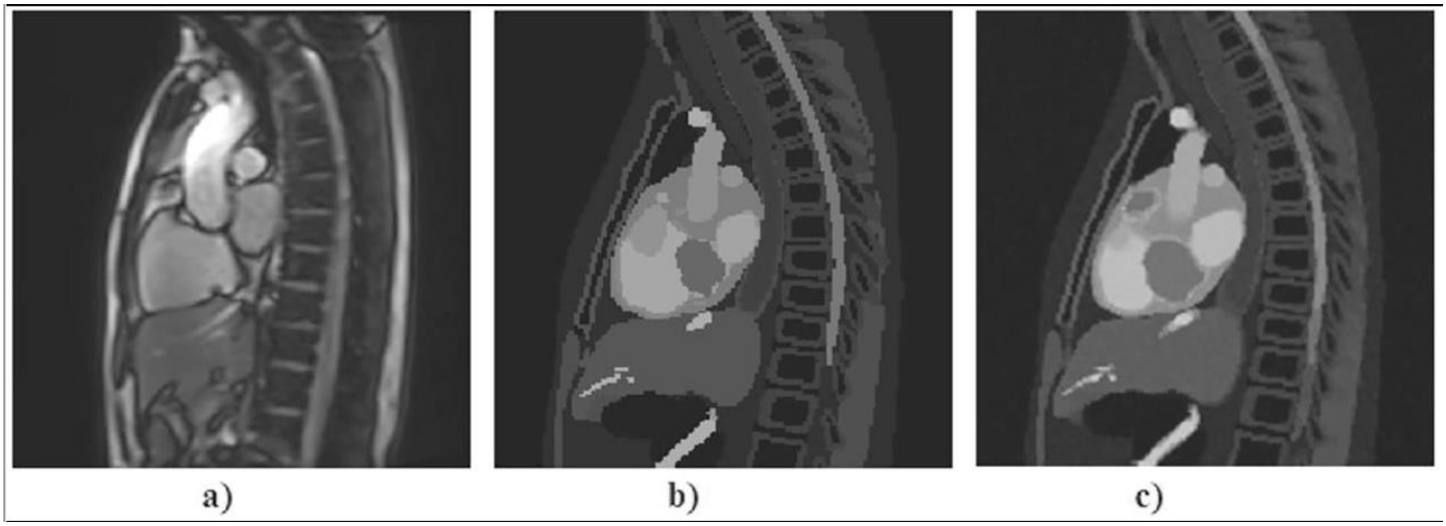

Fig. 2. Sagittal slice orientation of a) a real-time sagittal plane from Ipsen et al. [14] b) an original MRI simulated XCAT phantom and c) inclusion of partial volume and noise effects.

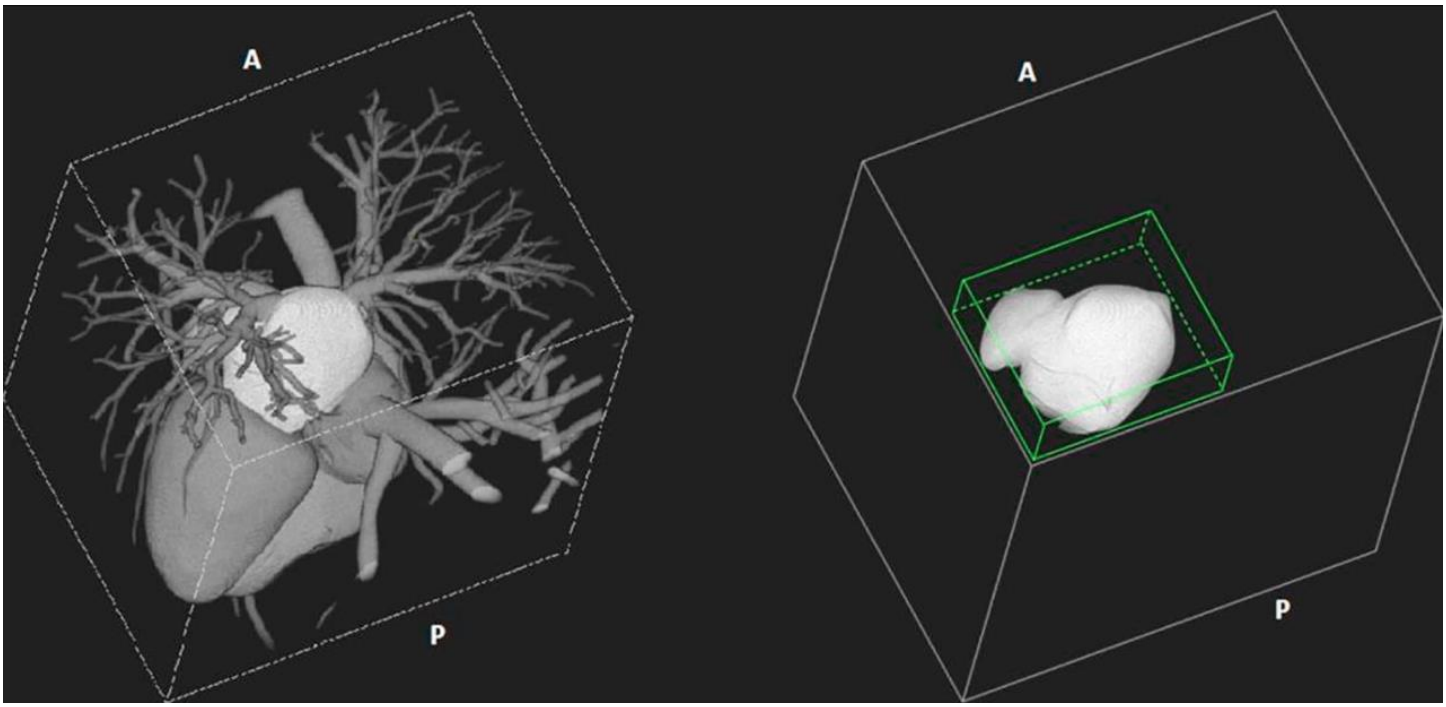

Fig. 3. (Left) 3D volume render of the XCAT cardiac model, lighter grey highlighting the target LA. (Right) The volumetric center coordinate of the bounding box, shown as the small green box, was calculated in each real-time frame as the ground-truth target position.

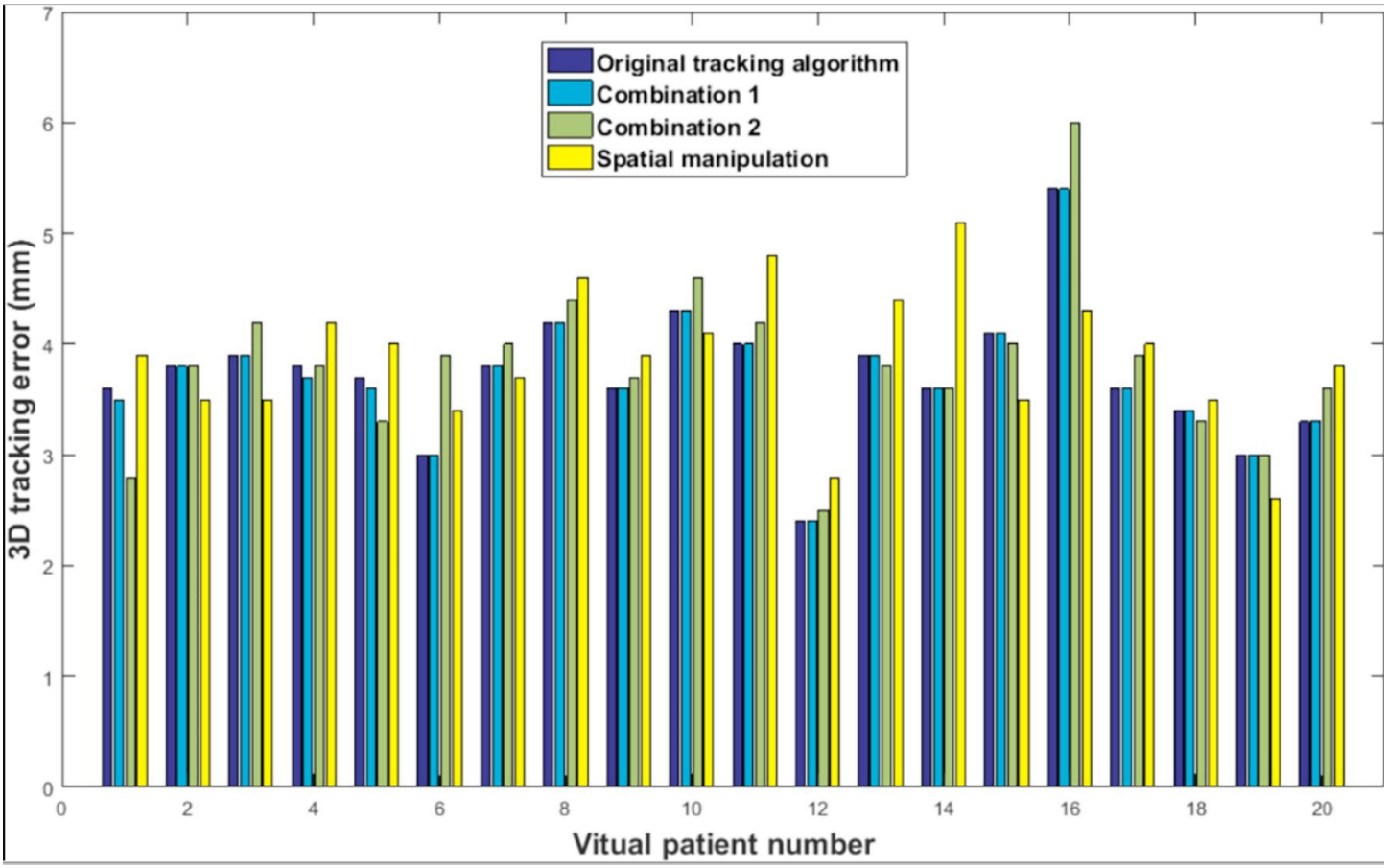

Fig. 4. Individual patients' 3D tracking errors across the 20 virtual patients for the original tracking algorithm and three scenarios of different tracking function combinations.

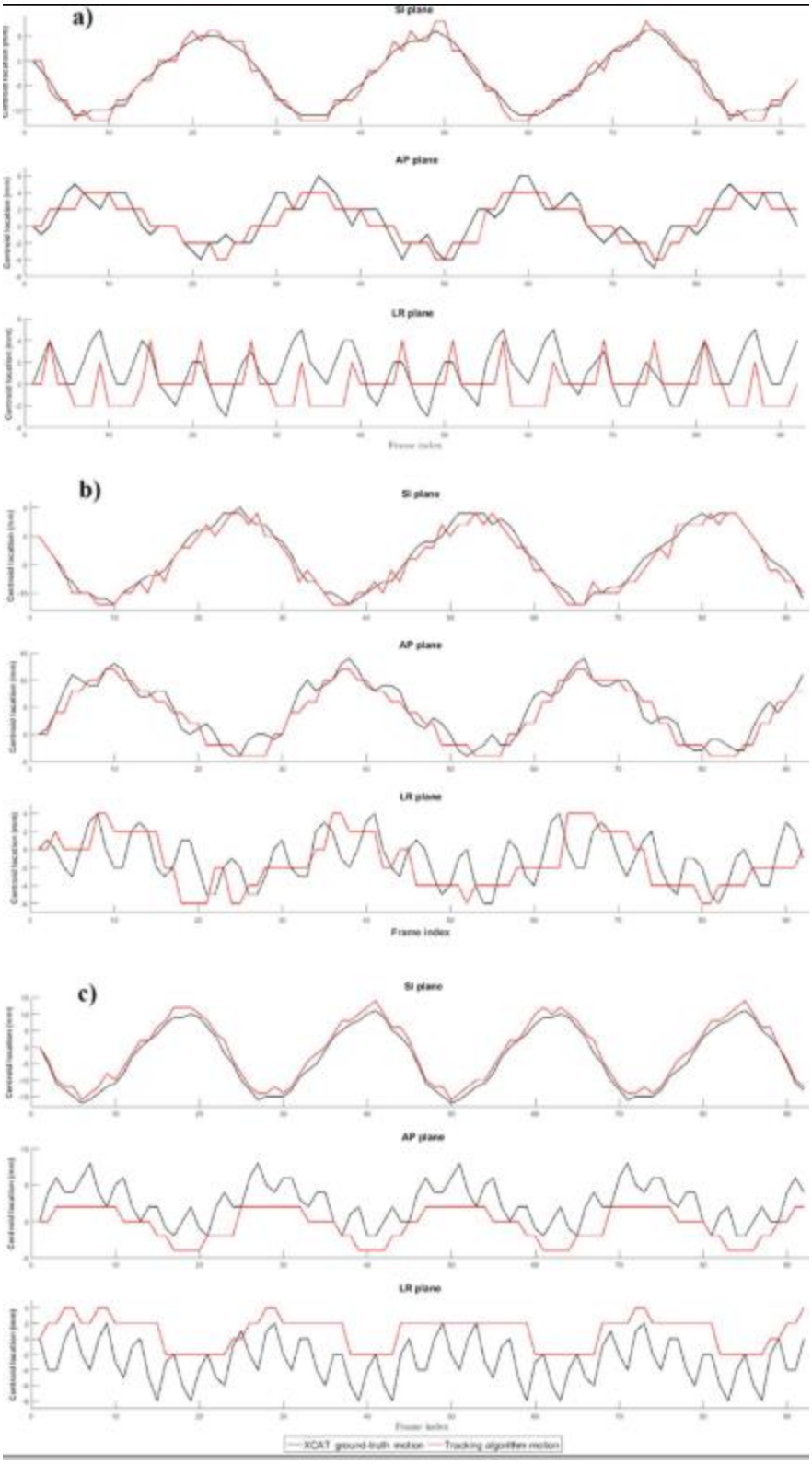

Fig. 5. Representative tracking performances for three virtual patients. Virtual patient 12 illustrates a best case scenario (a). Virtual patient 14 illustrates an average case (b) and virtual patient 16 illustrates a worst case tracking performance (c).